Precise Machining Based on Ritz Non-uniform Allowances for Titanium Blade Fabricated by Selective Laser Melting

Bo Zhang
Nanjing University of Science and Technology
Juntang Yuan
Nanjing University of Science and Technology
zhenhua wang (niatwzh17@163.com)
Nanjing University of Science and Technology
Xi Li
Nanjing University of Science and Technology

Research Article

Keywords: Precise machining, Selective Laser Melting, Blade, Ritz non-uniform allowance, Ti-6Al-4V alloy

Posted Date: June 8th, 2021

DOI: https://doi.org/10.21203/rs.3.rs-575906/v1

Version of Record: A version of this preprint was published at The International Journal of Advanced Manufacturing Technology on January 18th, 2022. See the published version at https://doi.org/10.1007/s00170-022-08701-7.

Precise Machining Based on Ritz Non-uniform Allowances for Titanium Blade Fabricated by Selective Laser Melting

Zhang Bo[1] •Yuan Juntang[1, *] • Zhenhua Wang[1, *] •Li Xi[1]

[1] School of Mechanical Engineering, Nanjing University of Science and Technology, Nanjing 210094, China

* Corresponding author. E-mail address: mc106@njust.edu.cn (Juntang Yuan),
niatwzh17@163.com (Zhenhua Wang).

Abstract

Selective Laser Melting (SLM) is an increasingly concerned trend in Ti-6Al-4V blade manufacturing, while the SLMed Ti-6Al-4V blade cannot be used directly because of poor surface integrity and high residual stresses. Precise machining after SLM is a feasible solution but also a challenge. The low rigidity of the blade will lead to deformation when machining. The deformation can lead to surface error and may make defect parts. Two-steps machining processes to address the problems were proposed in this paper. First, a non-uniform allowance distribution was allocated and optimized in semi-finishing based on Ritz solution to elastic deformation. The blade was simplified as a cantilever thin plate with various thickness, and the thickness of finishing allowance was designed and optimized on the premise of ensuring the thin-wall stiffness of the blade, so as to realize the design of Ritz non-uniform allowance. Then, finishing machining was conducted to achieve precise parts. A blade deformation model was established to evaluate surface error with cutting force moving and changing. Finite element analysis and experimental validation in ball-end milling of a blade were conducted. FEA results and experimental results showed dimensional errors have been reduced up to 50%. Further surface tests demonstrated that the mean surface roughness reduced from 7.88 μm to 0.815 μm. And the residual surface stresses of the SLM samples changed after semi-finishing machining due to the residual stress relaxation and redistribution. The results demonstrated that the proposed method enhanced the surface quality of blade fabricated by SLM.

Keywords Precise machining; Selective Laser Melting; Blade; Ritz non-uniform allowance; Ti-6Al-4V alloy

1. Introduction

Additive manufacturing (AM) is a rather new type of metal parts manufacturing technology developed in recent years. Selective laser melting (SLM) is a typical common AM technology. It is a powder layer fusion technology that can produce complex structures with relatively good surface quality [1]. Ti-6Al-4V titanium alloy is a common SLM forming material. It has high strength to weigh ratio, high corrosion resistance and good performance at elevated temperatures, and has been widely used in aerospace field [2]. However, the surface quality and the manufacturing tolerances of Ti-6Al-4V parts built with SLM still require finishing processing to produce the final products. Furthermore, SLM is known to generate tensile residual stresses during the building process, while machining is an optional operation to change from tensile stress to compressive stress. At the same time, most workpieces fabricated by SLM are thin-walled parts. The cutting forces in the process of machining tend to produce unnecessary deformation, resulting in surface error of machined parts (see Fig. 1). The post machining accuracy must be considered for SLM forming components. The surface error prediction is necessary before machining. Some methods can be adopted to keep the error within a certain tolerance range. For different methods to improve the machining accuracy, modeling and simulations to predict the machining surface error are useful in verification before expensive experimental tests [3]. Some strategies are listed for improve the final surface topography [4]:

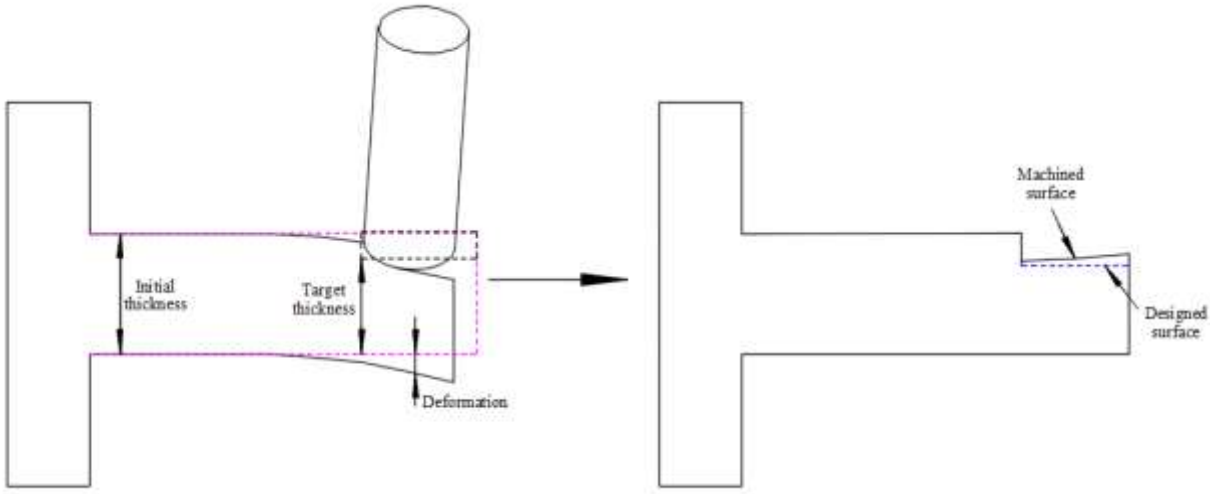

Fig. 1 Deformation and surface error during thin-wall parts machining.

(1) Changing machining strategy. Limiting cutting forces and adding sacrificial stiffeners can

increase minimum stiffness, but they often lead to inefficient productivity [5].

(2) On-line error compensation. The surface after machining is measured online in real time, and the subsequent processing is modified. Because the machine tool cannot respond to the adjustment in real time, this method has the problem of time delay, which also affects the machining efficiency [6].

(3) Off-line error compensation. Numerical methods are commonly used to predict and simulate the deformation of parts and tools in the process of machining. Compensations for deformation are conducted to improve the machining accuracy.

Although there is a certain deviation between the simulation results and the experimental results, which is due to the incompleteness of the factors considered, off-line error compensation is still a rather better choice based on productivity and usability. Many researchers pay attention to the off-time deformation modelling, error control, and compensation of thin-walled parts.

Song et al. [7] and Shi et al. [8] established a mathematical model for predicting the machining deformation of complex thin-walled structural such as blades by introducing the Rayleigh-Ritz solution. Wu et al. [9] predicted the deformation in thin-walled frame parts based on the finite element model and proposed two methods, large depth of cut and tool path optimization in thin-walled parts. Chen et al. [10] proposed a layered complete compensation and multiple iterative optimization compensation methods for aeronautical annular thin-walled parts to compensate for machining errors caused by machining deformation. They [11] also used multi-layer cutting to improve the machining accuracy of thin-walled parts. Tian et al. [12] performed eigenvalue sensitivity analysis on each position of the thin-walled flat piece to obtain the machining vibration-sensitive area of the workpiece. The characteristic sensitivity analysis and the non-uniform residual distribution were performed to obtain the semi-finished blank workpiece. The test showed that the method has a better control effect on machining vibration and machining deformation and can obtain better surface quality. Shan et al. [13] adopted linear variation sinusoidal trigonometric function based on the geometric shape of the workpiece, the non-uniform margin design of the cantilever direction and the cross-section direction of the blade. Rahman et al. [14] used a three-dimensional volumetric error model to describe two methods for modifying NC programs for machine tool modelling and measurement. Ratchev [15] and Guo [16] set the establishment of the cutting force model and used elastic mechanics and finite element calculation

analysis method to calculate the elastic deformation of thin-walled parts during machining.

In this paper, a Ti-6Al-4V titanium alloy blade was taken as the research object to solve poor surface quality after SLM processing. The error caused by the deformation of the thin-walled parts during the machining process was obtained. Because of residual stresses in SLM parts, there was potential distortion in machining with the release of residual stresses. Two-steps machining strategies were proposed to get a precise workpiece. The two-step machining processes were proposed by performing the roughing - semi-finishing - finishing processes. A semi-finish was conducted to get the non-uniform semi-finished product based on the proposed Ritz solution in the first step. In the second step, finishing machining was conducted to get the final surface.

2. Non-uniform allowances based on machining error prediction model

The blade, one of the most important thin-walled parts, is widely used in aerospace and aeronautic industries, and it is common components in SLM. The purpose of this section is to establish a mathematical model to predict the surface error of blades with complex shape during the milling process after SLM, then a non-uniform allowances are allocated based on the Ritz solution.

The following assumptions are made to simplify the calculation of defined the thin-walled blade workpiece [17]:

(1) Milling cutter and the fixture can be considered rigid, and the material of the workpiece is isotropic;

(2) The deformation of the blade is considered as pure elastic deformation;

(3) The milling force loaded on the blade is converted to the concentrated force moving along the feed direction;

(4) There is no initial stress in the workpiece.

The finished surface is generated by the cutter swept envelope. For a given cutting point, the dimensional surface errors are equal to the elastic displacements caused by the cutting force.

The surface error of the whole blade is determined by the normal distance between the surface swept by the cutter and the rebounded surface after machining. Since the surface errors are measured as the normal deviations between the actual machined surface and the designed surface, the predicted errors are equal to the elastic deformation in every machined area [18].

2.1 Deformation prediction mathematic model

For a complex blade, it can be simplified as a thin cantilever plate. Fig. 2 shows the geometry of the blade and its simplified thin cantilever plate used in this paper, respectively. As seen in Fig. 2, the blade has a twisted surface with various thickness along the length and height. The blade becomes a cantilever plate with varying thickness after it is flatted. The thin cantilever plate is clamped at one edge and other edges are free (Clamped-Free-Free-Free plate).

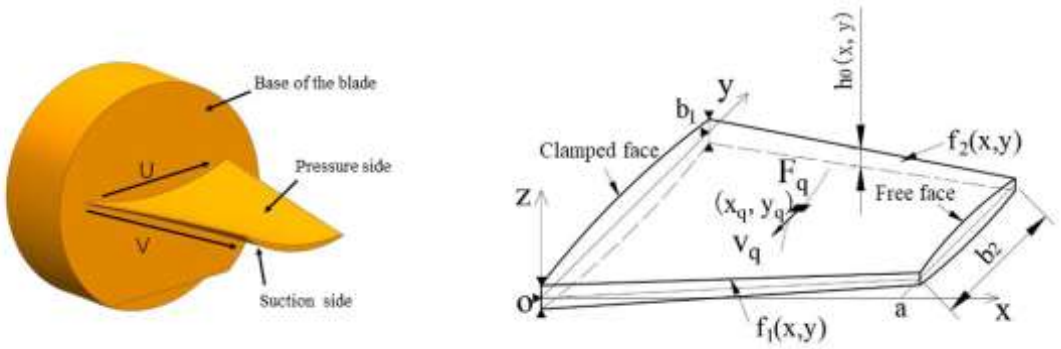

Fig. 2 Blade model and its simplification

For the blade, the stiffness in the lateral direction is much higher than in the perpendicular direction. The surface error after milling is mainly determined by the perpendicular deformation. The governing equation of thin-wall deformation is a fourth-order partial differential equation. The differential equation based on Kirchhoff's assumptions can be expressed as formula 1 by a transversal deflection [19] :

$$D\left(\frac{\partial^4 w}{\partial x^4} + 2\frac{\partial^4 w}{\partial x^2 \partial y^2} + \frac{\partial^2 w}{\partial y^4}\right) - q = 0 \quad (1)$$

Where, *w(x, y, t)* is displacement of plate at any *(x, y)* at any particular time, *q* is the external load, $\mathrm{D} = \mathrm{Eh}^3/[12(1-\mu^2)]$. Where *E* is Young's modulus of plate, *h* is Thickness of plate, and *v* is Poisson's ratio for plate material.

A typical solution for formula 1 is shown as formula 2, based on our previous research.

$$w = \left(C_1 + C_2 \sin\frac{\pi y}{2b\sqrt{2-\mu}} + C_3 \cos\frac{\pi y}{2b\sqrt{2-\mu}}\right)\left(1 - \cos\frac{\pi x}{2a}\right) \quad (2)$$

Where, a and b are the length *v*-direction and *u*-direction along of the plate, respectively; *D* is the flexural stiffness of the plate depending on the plate thickness and material properties. The undetermined coefficients *C1*, *C2* and *C3* are determined by external load and boundary conditions.

2.2 Ritz solution for solving blade surface error

Ritz energy solution is used to solve the simplified equations. The Ritz solution [20] is based on the principle of minimum potential energy. The true displacement of the system is obtained by solving the displacement that minimizes the system's potential energy. For the thin-walled part cutting system, the total potential energy of the system can be divided into the strain energy *U* of the deformed blade and the virtual energy *V* generated by the cutting force, as shown in formula 3 to formula 5:

$$\Pi = \mathrm{U} + \mathrm{V} \tag{3}$$

$$U = \frac{D}{2}\iint\left\{\left(\frac{\partial^2 w}{\partial x^2}+\frac{\partial^2 w}{\partial y^2}\right)^2 - 2(1-\mu)\left[\frac{\partial^2 w}{\partial x^2}\frac{\partial^2 w}{\partial y^2} - \left(\frac{\partial^2 w}{\partial x \partial y}\right)^2\right]\right\}dxdy \tag{4}$$

$$V = -\iint qwdxdy \tag{5}$$

Based on the minimum potential energy theorem, a discrete solution using the Ritz energy solution was proposed. For a specific machining point $(\mathrm{x_c}, \mathrm{y_c})$, seen in Fig. 3, the strain energy *U* can be calculated by formula 6.

$$U(x_\mathrm{c}, y_\mathrm{c}) = \frac{E}{24(1-\mu^2)}\left\{\int_{f_1}^{f_2}\int_{x_\mathrm{c}}^{a} h'^3\delta dxdy + \int_{y_\mathrm{c}}^{f_2}\int_{x_\mathrm{c}-a_\mathrm{e}}^{x_\mathrm{c}} h'^3\delta dxdy + \int_{f_1}^{y_\mathrm{c}}\int_{x_\mathrm{c}-a_\mathrm{e}}^{x_\mathrm{c}} h^3(x,y)\delta dxdy + \int_{f_1}^{f_2}\int_{0}^{x_\mathrm{c}-a_\mathrm{e}} h^3(x,y)\delta dxdy\right\} \tag{6}$$

Where f_1 and f_2 are the boundaries of blade along *u* direction, a_e is the length of discrete area which is to be machined in processing. *h* is the thickness of blade and h' is the machined thickness of blade.

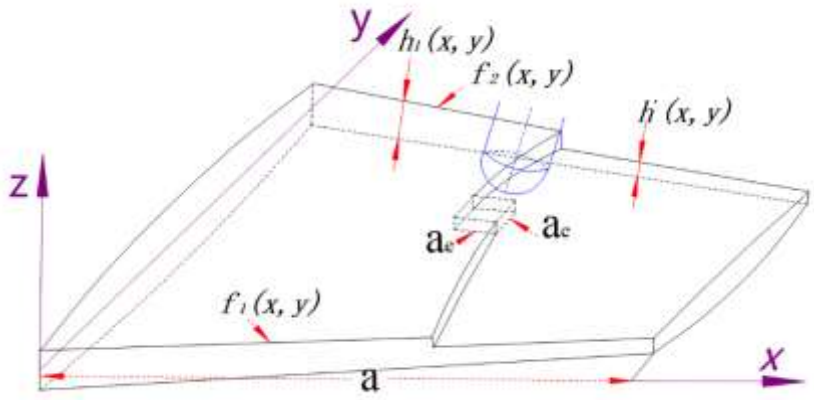

Fig. 3 Diagram of deformation in simplified blade machining.

According to the measure data, formula 7 are fitted for two edges. According to Table 1, the fitting model of blade thickness at each position, seen in Fig. 4, is shown in formula 8. The fitting accuracy R^2 is 0.97, which proves an acceptable fitting degree.

$$\begin{cases} f_1: \ y = 0.10998x \\ f_2: \ y = -0.10998x + 36.66 \end{cases} \tag{7}$$

$$h(x,y) = (1 - 0.006x)\left[-0.0042\left(\frac{y-18.33}{1-0.006x}\right)^2 + 0.0011\left(\frac{y-18.33}{1-0.006x}\right) + 2\right] \tag{8}$$

The thickness of machined surface was calculated as $h'(\mathrm{x},\mathrm{y}) = h(\mathrm{x},\mathrm{y}) - a_p$, a_p is the set depth of removal material, where the deformation caused difference assumed to be negligible.

Table 1. Thickness of each position in SLM blade.

x-axial/mm	ratio along U-direction(Y-axial)										
	0	1/30	3/30	6/30	10/30	15/30	20/30	24/30	27/30	29/30	1
0	0.598	1.102	1.495	1.782	1.953	2.009	1.953	1.782	1.495	1.102	0.598
14	0.548	1.010	1.370	1.632	1.788	1.841	1.788	1.632	1.370	1.010	0.548
28	0.498	0.917	1.244	1.482	1.624	1.672	1.624	1.482	1.244	0.917	0.498
38	0.462	0.851	1.154	1.376	1.507	1.551	1.507	1.376	1.154	0.851	0.462
44	0.440	0.811	1.100	1.311	1.437	1.479	1.437	1.311	1.100	0.811	0.440
48	0.426	0.785	1.065	1.269	1.390	1.431	1.390	1.269	1.065	0.785	0.426
50	0.419	0.772	1.047	1.247	1.367	1.407	1.367	1.247	1.047	0.772	0.419

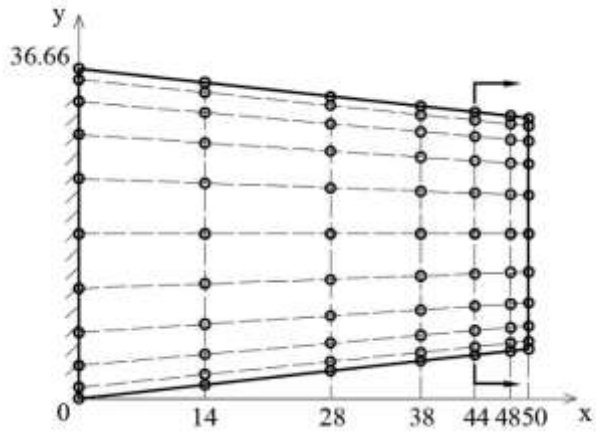

Fig. 4 Diagram of thickness in simplified blade.

Then, virtual work *V* is calculated by the work done by the cutting force, as seen in formula 9.

$$V(x_c, y_c) = \int_{y_c - a_e}^{y_c} \int_{x_c - a_e}^{x_c} \frac{F_n}{a_e} w(x,y)\,dx\,dy \tag{9}$$

The following equations are based on the Ritz solution, where the variables *C1*, *C2* and *C3* were calculated.

$$\frac{\partial \Pi(x_c, y_c)}{\partial C_1} = 0, \ \frac{\partial \Pi(x_c, y_c)}{\partial C_2} = 0, \ \frac{\partial \Pi(x_c, y_c)}{\partial C_3} = 0 \tag{10}$$

Substitute back *C1*, *C2* and *C3* in the assumed solution and each cutting time-domain

deformation response of the plate is obtained.

2.3 Milling force-deformation coupling prediction model

The effect of deflections for actual cutting forces is not neglected, so an iterative correction algorithm is developed to ensure computation reliability and accuracy. Research results showed that cutting forces were the dominant factors that cause elastic deformation during the machining process. In this study, the force is only related to the selection of machining parameters. The real-time change of cutting force caused by cutting edge cutting is not considered.

The coupling relation between cutting forces and machining deformation is taken into account. Hence an iteration cutting force algorithm is conducted. The cutting force is modelled as a moving load along the feed direction to simulate the tool moving along the length of the developed model. The milling force along the normal to the feed direction becomes perpendicular load acting on a thin cantilever plate workpiece. A Kistler piezoelectric dynamometer (5698A) was used for machining force measurement to simulate the milling force in the developed model. For blade machining, incline angular is constant so that the calculated cutting force was effective. The incline angular in this paper is set to 20° [21], as seen in Fig. 5. The parameter of experiments is shown in Table 2. An exponent cutting force model was used for force calculation. The fitting model was showed as formula 11. Due to the influence of deformation, the actual cutting depth is less than the designed cutting depth. Therefore, the interpolation method is used to solve the depth of the actual machining iteratively, when the thickness error of the two steps is less than 1 μm, the iteration ends.

$$\begin{cases} F_{\mathrm{x}} = 6.2840 n^{0.2011} {f_z}^{0.1391} {a_p}^{0.5657} p^{0.1208} \\ F_{\mathrm{y}} = 49.879 n^{0.1318} {f_z}^{0.3518} {a_p}^{0.7156} p^{0.1804} \\ F_{\mathrm{z}} = 92.278 n^{0.1147} {f_z}^{0.3719} {a_p}^{0.2572} p^{0.5242} \end{cases} \tag{11}$$

The discrete allowance elements were faired linearly. The blank model with a non-uniform allowance can be obtained as shown in Fig. 6. Non-uniform allowance allocation based on the above method for the finishing of the SLM titanium blade is allocated. The distribution of the allowance is shown in Table 3. As seen in the Fig. 6, the maximum allowance is 1 mm while the minimum is 0.2 mm.

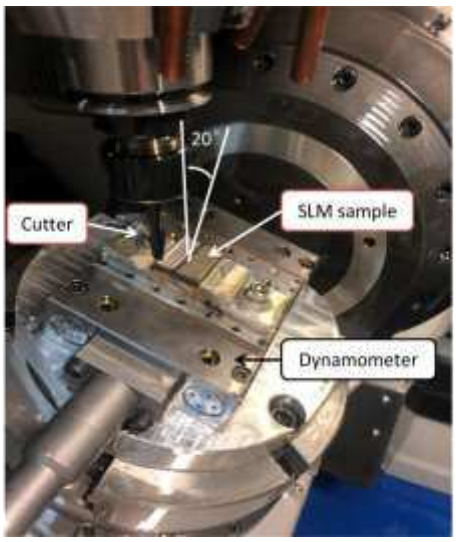

Fig. 5 Machining force measurement process.

Table 2. Cutting force experiments.

Cutting speed n(r/min)	Feed f_z (mm/z)	Cutting axial depth a_p (mm)	Pitch p (mm)	F_x (N)	F_y(N)	F_z(N)
4000	0.01	0.1	0.1	3.934	4.033	14.28
6000	0.03	0.1	0.3	5.296	7.313	32.94
7000	0.04	0.1	0.5	6.465	8.465	54.04
5000	0.02	0.1	0.7	5.079	6.089	51.20
6000	0.04	0.25	0.1	8.175	14.44	26.25
4000	0.02	0.25	0.3	7.408	11.88	31.24
5000	0.01	0.25	0.5	6.626	9.082	38.70
7000	0.03	0.25	0.7	8.786	14.59	55.72
7000	0.02	0.4	0.1	9.667	16.18	26.89
5000	0.04	0.4	0.3	10.81	22.96	39.12
4000	0.03	0.4	0.5	11.29	21.52	51.58
6000	0.01	0.4	0.7	10.77	14.63	41.36
5000	0.03	0.55	0.1	10.22	11.55	17.55
7000	0.01	0.55	0.3	13.52	18.08	33.48
6000	0.02	0.55	0.5	15.20	24.15	46.52
4000	0.04	0.55	0.7	16.42	32.57	66.92

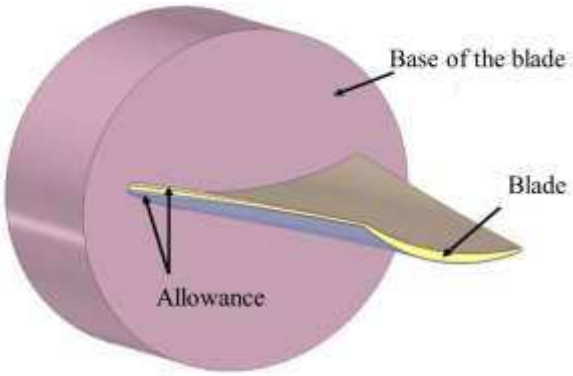

Fig. 6 Model of semi-finished workpiece with Ritz non-uniform allowance.

Table 3. Non-uniform allowance of each position in SLM blade.

x-axial/mm	ratio along *u*-direction(*y*-axial)										
	0	1/30	3/30	6/30	10/30	15/30	20/30	24/30	27/30	29/30	1
0	1	1	1	1	1	1	1	1	1	1	1
14	1	1	1	1	1	1	1	1	1	1	1
28	0.49	0.55	0.614	0.7	0.746	0.7	0.614	0.55	0.49	0.436	0.49
38	0.294	0.318	0.344	0.374	0.39	0.374	0.344	0.318	0.294	0.276	0.294
44	0.246	0.26	0.274	0.29	0.3	0.29	0.274	0.26	0.246	0.234	0.246
48	0.224	0.238	0.254	0.264	0.274	0.264	0.254	0.238	0.224	0.216	0.224
50	0.21	0.22	0.232	0.246	0.26	0.246	0.232	0.22	0.21	0.2	0.21

3. Methodology

3.1 SLM progress

The SLM blade samples were built using MLab Cusing machine M2 from CONCEPT LASER. Ti6Al4V powders were prepared as the bed powder fusion to form the samples. The chemical composition of the powder is listed in Table 4. The Processing parameters were adjusted to be optimized according to the previous studies, as seen in table 5. No further changes to the process parameters were made during the build process. Fig. 7 shows the samples fabricated. The designed blade has a height of 50 mm, and the thickness varies from 1.99 mm to 2.88 mm. Note that in this case, the base of the built titanium blade has one plat step to make it easier to perform accurate machining and measurements. Once the SLM forming was finished, the parts were cleaned and stress relieved according to the specification.

Table 4. Chemical composition of Ti-6Al-4V(mass fraction, %)

Al	V	O	Fe	C	N	H	Ti	Others
5.5-6.75	3.5-4.5	0.13	0.14	0.007	0.007	0.002	Bal.	<0.05

Table 5. Process parameters used in fabricating SLM Ti-6Al-4V samples.

Process parameters	Values
Laser power	180W
Scanning speed	1200mm/s
Laser spot diameter	150μm
Hatch spacing	105μm
Layer thickness	30μm

Fig. 7 Blade samples fabricated by SLM.

3.2 Machining experiments

The semi-finishing and finish machining were conducted with a 5-axis CNC milling machine (Willemin 408S2). The two-fluted carbide ball end with a diameter of 6 mm and a helix angle of 30° was used to cut SLM samples, the same kind of tools used in section 2.3. The tool paths for the five-axis milling of the blade were generated with HyperMill software using a 5X-ISO module. Machining tests were carried out with oil coolants. In addition, a ruby probe was used to calibrate the benchmark plane of the finishing machining. Other than allowances, the machining conditions for the two samples were the same.

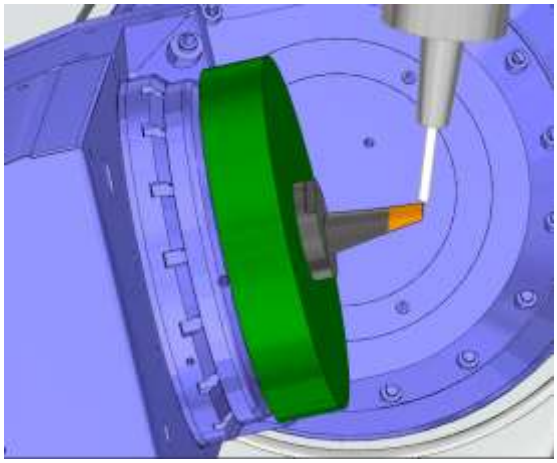

Fig. 8 Diagram of 5-axis milling.

Two-steps machining processing was carried out to obtain a better machining quality. An optimum non-uniformed blank with calculated allowance was achieved in the first step. The blade geometries after semi-finishing with two different allowance were used for comparison. Uniform blade geometry had identical allowances of 0.6 mm. The Ritz allowances were generated with the continuous envelope surface by connecting the discretely non-allowance allowance, according to section 2.3. A spline curve connects each point. A traditional machining strategy was applied to fulfil the final machining in the second step.

3.3 Finite elements method verification

The finite element analysis (FEA) approach can be used for surface error prediction. In this paper, surface errors were caused by elastic deformation, so FEA is also a method for surface errors verification. To verify the proposed Ritz method, FEA was used to compare the surface error produced by different allowance allocation. The geometry model of the blade was imported into the Ansys software, and the coordinate system in Ansys software was consistent with the coordinate design system of the blade. Material attributes of SLM Ti-6Al-4V alloy used in the FEA were Young's modulus of 110 GPa, the density of 4430 kg/ m^3 and Poison's ratio of 0.3. Efficient hexahedral units were used to divide the grids [18]. The FE model of the initial workpiece was built with a fixed constraint to the blade bottom surface. Cutting force was loaded using the APDL*Model Change keyword. The elemental cutting forces were then equally distributed into the grid nodes involved in the swarf region. Meanwhile, these forces were all described in the $OX^0Y^0Z^0$ coordinate system. Thus, after the deformation of the workpiece was computed, the spatial displacements of the grid nodes should be converted into the OXYZ coordinate system for iterative

computation, shown in Fig 9. The whole analysis process is shown in Fig. 10. During the simulation of machining, the removal of material was realized through the concept of element death in FEA software. Addition to uniform allowances and Ritz non-uniform allowances, sinusoidal allowances as one more non-uniform allowance was analyzed for comparison.

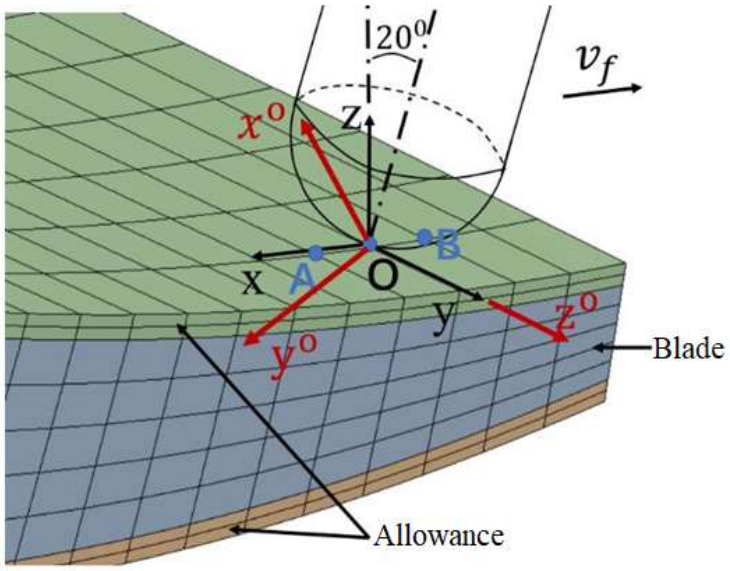

Fig. 9 Diagram of coordinate transformation.

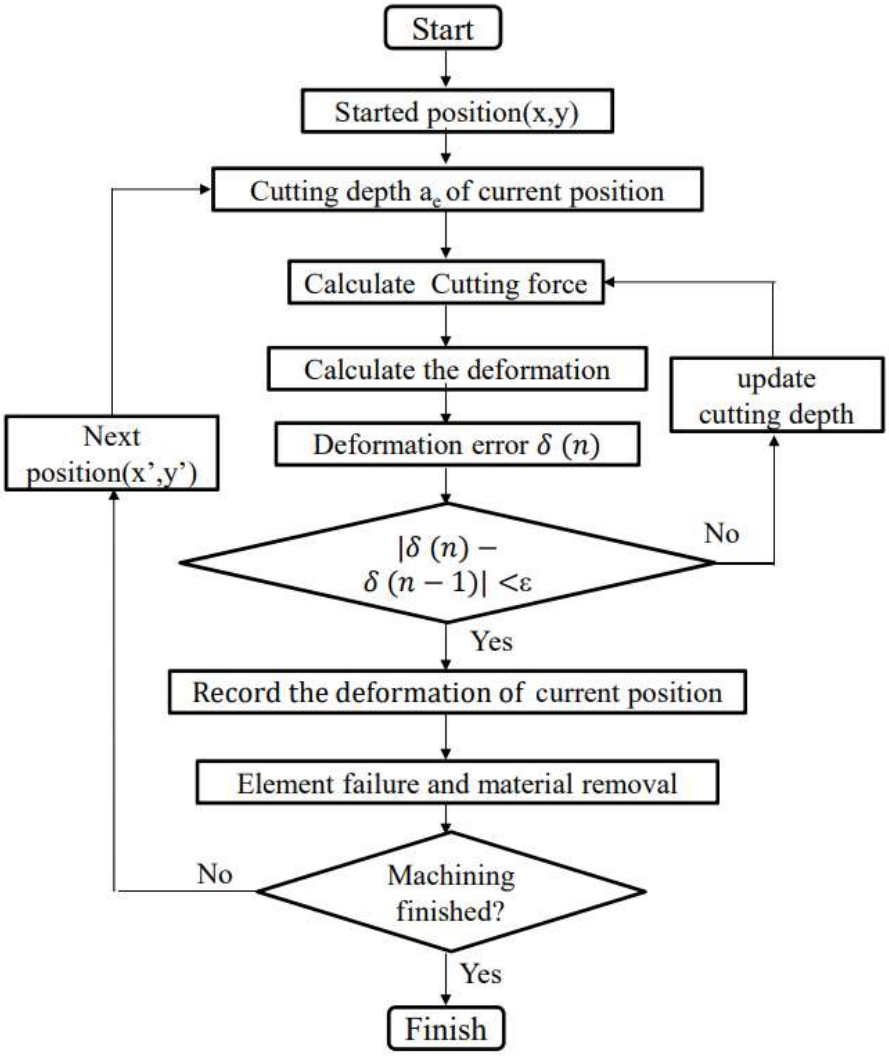

Fig. 10 Flow chart of finite element analysis.

3.4 Result measurement

3.4.1 Surface error measure

The surface displacement profiles of the two allowance allocate samples were measured with a HEXAGON coordinate measuring machine by using a 1.5-mm-diameter touch probe. The measurements were carried out in the temperature-controlled room with a temperature of 20 ℃. The machining error was calculated considering the distance between the measurement points and locations of the 3D designed model. The predicted surface errors at 5×7 sampled points on the designed surface were compared with the experimental measurement. The measure points located on or close to the boundaries were not considered to avoid unwanted measure uncertainties.

3.4.2 Residual stress measurement

Residual stresses in the machined parts were measured using the X-ray diffraction technique, consisting of determining the variations in peak positions due to distortions of the crystalline lattice. The measurements were performed using X-350A residual stress measurement system with a portable MG40P standard Ψ-2θ goniometer. The parameters used in the X-ray analysis are shown in Table 4.

Table 4. Parameters used in the X-ray Analysis of Ti-6Al-4V

Parameters	value	Parameters	value
Test material phase	α-Ti	Ψ angular	0°, 24.2°, 35.3°, 45°
Wavelength radiation	$Cu-K\alpha$	Filter	V
Bragg angle 2θ	137°-147°, (hkl)=(213)	Voltage	22KV
Stress Constance	-277MPa	Current	6mA
detector position Changing	0.1°	Collimating tube diameter	3mm

3.4.3 surface roughness measurement

The average surface roughness (R_a) was taken in account for the present research. The roughness of machined surface mainly depends on the row spacing direction relative to the machining. The surface roughness was measured by using an ISR-S400 5-μm stylus type instrument from INSIZE. The measurement were conducted five times, and a mean value was taken for final results.

4. Result and discussion

The machined blades are shown in Fig.11. The surface topography was obviously different between before and after machining processes. The machined surface roughness of blades with uniform allowance and Ritz allowance were 0.854 μm and 0.815 μm, respectively, while the roughness of the as-built surface was 7.88 μm.

Fig. 11 Blade samples after SLM. (a) Blade before machining, (b) Machined blade with Ritz allowance, (c) Machined blade with uniform allowance

4.1 FEA results

The simulated deformations of the blade with three different allowances after milling are shown in Fig. 12. The surface error of uniform allowance was larger than that of the other two non-uniform allowances. The largest error area of the blade was mainly located on the tip of the blade. The relative stiffness of the two tips of the blade was small and the deformation was large. The deformation decreases until the base of the blade along *v*-direction. The relative stiffness of the blade was high at the base of blade. As seen in Fig. 11, the dimensional surface errors of the blade first increased and then decreased nonlinearly along the *u*-direction. The maximum deformation of the uniformed blade was 0.1940mm, while the ones of sinuous allowance and Ritz allowance were 0.1165mm and 0.0748mm, respectively. It showed that the magnitude of the machining errors with a non-uniform allowance can be significantly reduced by at least 62% compared to errors with uniform allowance. Also, it shows that the precision of the thin-walled blade with non-uniform allowance strategies were greatly improved. The finite element simulation results showed that, compared with the traditional uniform allowance distribution method, the non-uniform allowance distribution method proposed in this paper could effectively ensure the stiffness of parts and reduce the surface error of parts. At the same time, the maximum error produced by proposed method was smaller than that produced by sinusoidal allowance in reference [12].

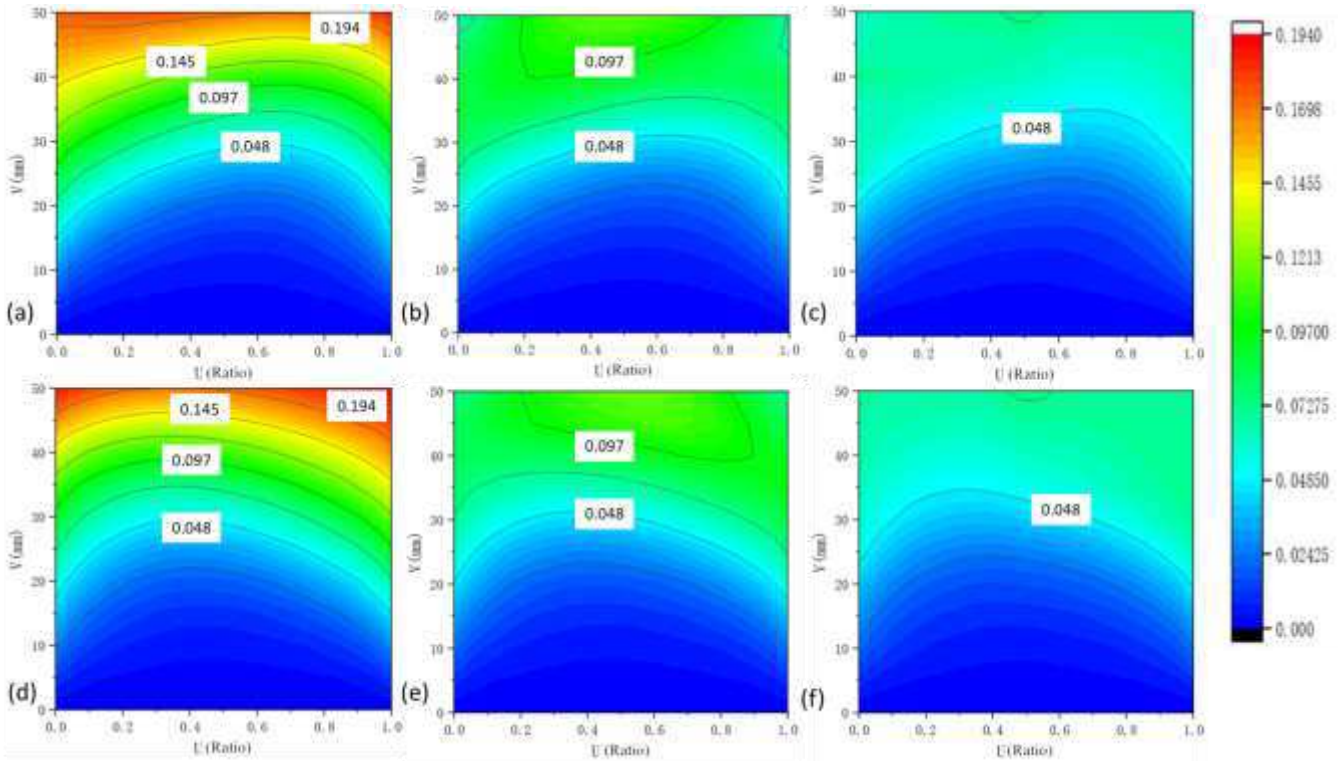

Fig. 12 Residual error of machined blade with 3 different allowances. (a) pressure error with uniform allowance (d) suction back error with uniform allowance, (b) pressure error with sinuous allowance, (e) suction error with sinuous allowance, (c) pressure error with Ritz allowance, (f) suction error with Ritz allowance.

4.2 Experiment results

The tool path started in the suction side on the blade top. So the maximum surface error was located in point 1 on line #1, as shown in Fig. 13(a). The maximum machined surface error resulting from the uniform allowance reached 0.30 mm. However, the machined surface error result from the proposed Ritz non-uniform allowance was about 0.15 mm. The machined surface errors were generally reduced by 50%. Three specific surface errors on both blades were compared along the tool path. The trend of the experimental surface errors of the blade sampling points along the *u* and *v* directions was in good agreement with the simulation results, but the relative magnitude of the errors was determined by a certain error. The maximum prediction error is 50%, and the average prediction error was 30%. Fig. 13 shows the comparison of the surface errors of the two kinds of allowance at the selected position on the blade, in which the surface errors of the line # 1 is along *v*-direction, the line # 2 and line # 3 are along the *u*- direction.

As illustrated in Fig. 13(b), the surface error decreased gradually along the *v* direction, consistent with the blade with uniform allowance. The two allowances showed the maximum

surface errors at the tip of the blade. By evaluating the stiffness of the transition state of each machining feature, the Ritz non-uniform allowance was distributed to ensure the stiffness requirements in the finishing process. The distribution tendency was consistent with the FEA results.

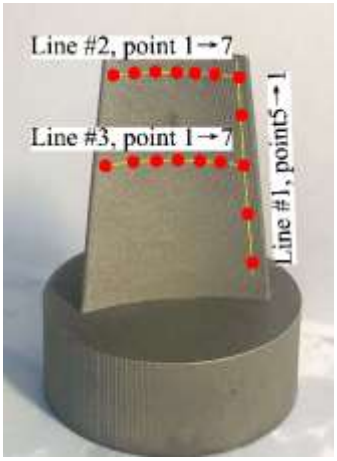

a) Schematic diagram of measure points.

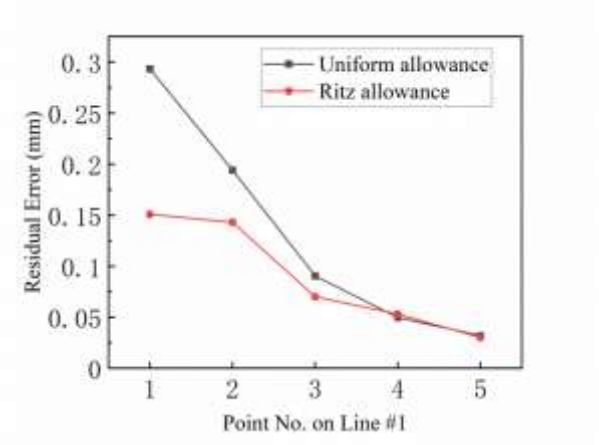

b) Results of line #1.

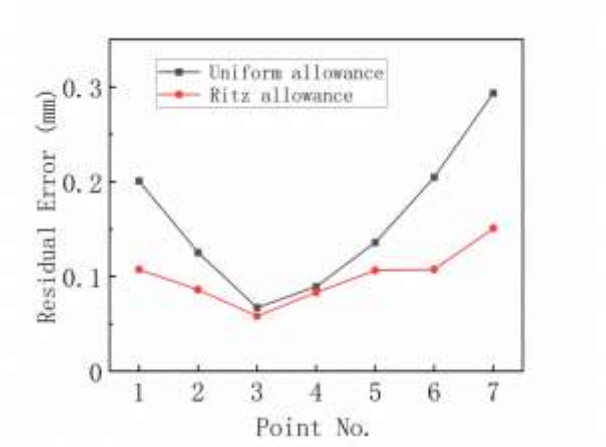

c) Results of line #2.

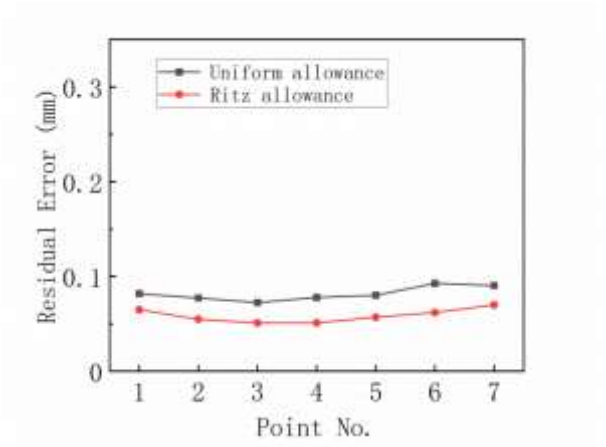

d) Results of line #3.

Fig. 13 Comparison of surface errors for milling of blades with uniform allowance and Ritz allowance.

Fig. 13 (c)-(d) compares and analyzes the surface errors of uniform allowance and Ritz allowance at the positions of v = 47 mm (# line 2) and v=30 mm (# line 3) along the feed direction. On v = 47 mm (# line 2), the surface error values of experiment and simulation showed a uniform nonlinear first decreasing and the increasing trend with the increase of the machining path along feed direction. Nevertheless, on v=30mm (# line 3), the variation along the feed direction was not as large as that near the blade tip, and the difference of relative maximum surface error was smaller.

The surface error results of the machined blade with non-uniform allowance based on the Ritz

method were presented and compared to that with uniform allowance. The deformation variation caused by the second-time machining decreased with the smaller cutting volume. Moreover, the initial and machining-induced residual stress could be released. Therefore, the experiments and FEA simulations validated the accuracy and effectiveness of the proposed model. Such results indicated that the proposed non-uniform allowance based on Ritz method for SLM parts could be used for high precision machining.

Nevertheless, the experimental results were not fully consistent with the results of FEA. The FEA results obtained with different allowance were smaller than the experimental ones measured by coordinate measuring machine. The cutting force, cutting heat, and the fixture load in the cutting experiments, which were not considered in the FEA model, were the main reasons for the error. Meanwhile, the errors introduced in three coordinate measurements could not be completely avoided, and most experimental methods and empirical models only showed a trend of the comparative results.

4.3 Residual stress results

As shown in Fig. 14, the residual stress at each point of the blade showed a certain difference. Fig. 14(b) shows the values of residual stress along the *v*-direction at five specific points of the machine blades and unmachined samples with Ritz non-uniform allowance. The values of residual stress along the *v*-direction increased with the distance from the base. Before machining, the residual stresses of the SLM sample were tensile, while the machined surfaces of both blades presented compressive residual stresses. As for the as-built SLM blade, with the increasing number of layers, heat accumulated in the formed layers, which reduced the temperature gradient in part. Hence, the tensile stress showed a trend that decreases from top to bottom. Consistent with the previous study, residual stresses on the top surfaces were compressive because the ploughing effect of cutting tools was obvious on the machined surface. The experimental results revealed the influence of the machining process on residual stresses. The machined effects to residual stresses could reach about 0.1 mm, as seen in Fig. 14(c).

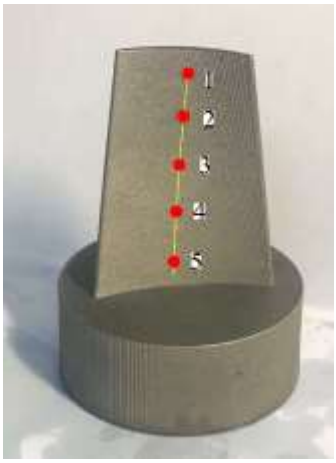

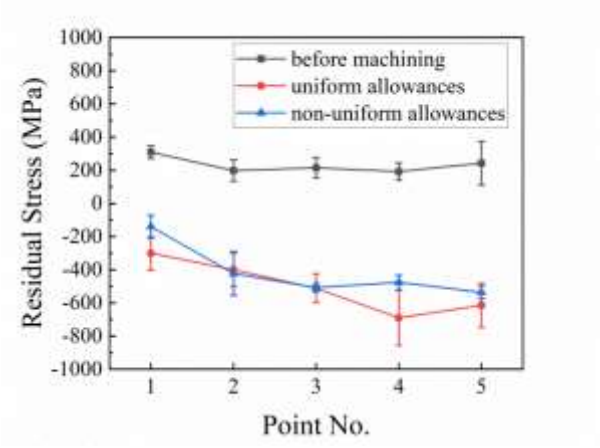

a) Schematic diagram of measure points b) Residual stress results of pitched points

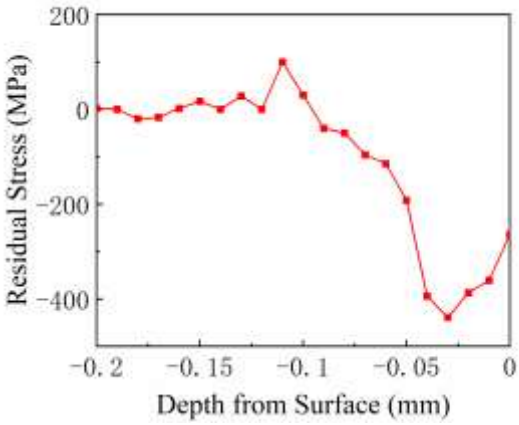

c) Residual stress results of pitched points along depth

Fig. 14 Residual stresses of blade with Ritz allowance after machined.

5. Conclusions

Blade parts fabricated by SLM have poor surface integrity and high residual stresses. In this paper, a novel machining strategy for Ti-6Al-4V blade parts fabricated by SLM was proposed. The surface errors caused by the elastic deflection were considered. A two-step machining strategy was proposed and proved to improve the machining accuracy and surface quality. FEM simulating and experiment validation were conducted to validate the efficiency of the proposed method. The main findings are summarized as follows:

1. SLM fabricated parts have poor surface and high tensile residual stresses. The average surface roughness is 7.88 μm. Tensile residual stresses range from 20 Mpa to 222 Mpa. Poor initial surface morphology and roughness of as-built Ti-6Al-4V sample result from melt traces and bonded

powders, high tensile residual stresses are related to fast cooling rate during SLM processing.

2. Ritz energy solution for thin wall deformation is suitable for predicting surface error. Compared to experiments validation, the prediction model has good consistent with experiment results. The non-uniform allowance based on the Ritz solution could decrease the surface error, the maximum surface error decreased by 50%, the Finite elements analysis and the experiment results showed the method could decrease the errors due to deformation.

3. Two-steps machining could improve the surface precision and better residual stresses. Residual stress after machining was compressive stress, which was beneficial when the fatigue strength of the blade was considered and hence was sought after. Meanwhile, better surface roughness of 0.815 μm were achieved.

4. The experimental validation showed that simulated modelling of machining deflections for the blade leads to an acceptable prediction of the dimensional surface errors. The present research provided the support for the potential application to achieve better surface quality for SLM blades. The non-uniform allowance method has been successfully implemented in the SLM blade milling, and its principle can be transferred to other thin-walled SLMed parts. Although the results are encouraging, the proposed method cannot eliminate surface errors. Moreover, the method may be unable to handle special parts, such as lattice parts. Further researches need to be explored.

Declarations

Funding This work was financially supported by the National Natural Science Foundation of China (No. 51675285).

Competing interests The authors declare no known competing interests.

Availability of data and material Not applicable

Code availability Not applicable

Ethics approval Not applicable

Consent to participate Not applicable

Consent for publication The authors gave consent for publication.

References

[1]Jiménez A, Bidare P, Hassanin H, Tarlochan F, Dimov S, Essa K. (2021) Powder-based laser

hybrid additive manufacturing of metals: a review. The International Journal of Advanced Manufacturing Technology,114:63-96. doi: https://doi.org/10.1007/s00170-021-06855-4

[2] Gurrappa I. (2003) Characterization of titanium alloy Ti-6Al-4V for chemical, marine and industrial applications. Materials Characterization,51:131-139. doi: https://doi.org/10.1016/j.matchar.2003.10.006

[3] Li Z, Tuysuz O, Zhu L, Altintas Y. (2018) Surface form error prediction in five-axis flank milling of thin-walled parts. International Journal of Machine Tools and Manufacture,128:21-32. doi: https://doi.org/10.1016/j.ijmachtools.2018.01.005

[4] Huang N, Bi Q, Wang Y, Sun C. (2014) 5-Axis adaptive flank milling of flexible thin-walled parts based on the on-machine measurement. International Journal of Machine Tools and Manufacture,84:1-8. doi: https://doi.org/10.1016/j.ijmachtools.2014.04.004

[5] Gao Y, Ma J, Jia Z, Wang F, Si L, Song D. (2016) Tool path planning and machining deformation compensation in high-speed milling for difficult-to-machine material thin-walled parts with curved surface. The International Journal of Advanced Manufacturing Technology,84:1757-1767. doi: https://doi.org/10.1007/s00170-015-7825-4

[6] Li Z, Zhu L. (2019) Compensation of deformation errors in five-axis flank milling of thin-walled parts via tool path optimization. Precision Engineering,55:77-87. doi: https://doi.org/10.1016/j.precisioneng.2018.08.010

[7] Song Q, Shi J, Liu Z, Wan Y. (2016) Dynamic analysis of rectangular thin plates of arbitrary boundary conditions under moving loads. International Journal of Mechanical Sciences,117:16-29. doi: https://doi.org/10.1016/j.ijmecsci.2016.08.005

[8] Shi J, Gao J, Song Q, Liu Z, Wan Y. (2017) Dynamic Deformation of Thin-walled Plate with Variable Thickness under Moving Milling Force. Procedia CIRP,58:311-316. doi: https://doi.org/10.1016/j.procir.2017.03.329

[9] Wu K, He N, Liao WH, Zhao W (2004) Study on machining deformations and their control approaches of the thin-web in end milling. China Mechanical Engineering 15(8):670–674.

[10] Chen W, Lou P, Chen H. (2009) Active compensation methods of machining deformation of thin-walled parts. Hangkong Xuebao/Acta Aeronautica et Astronautica Sinica,30:570-576.

[11] Chen YZ, Chen WF, Liang RJ, Feng T. (2017) Machining Allowance Optimal Distribution of Thin-Walled Structure Based on Deformation Control. Applied Mechanics and

Materials,868:158-165. doi: https://doi.org/10.4028/www.scientific.net/AMM.868.158

[12] Tian W, Ren J, Wang D, Zhang B. (2018) Optimization of non-uniform allowance process of thin-walled parts based on eigenvalue sensitivity. The International Journal of Advanced Manufacturing Technology,96:2101-2116. doi: https://doi.org/10.1007/s00170-018-1740-4

[13] Shan C, Zhao Y, Liu W, Zhang D. (2013) A nonuniform offset surface rigidity compensation strategy in numerical controlled machining of thin-walled cantilever blades. Hangkong Xuebao/Acta Aeronautica et Astronautica Sinica,34:686-693.

[14] Rahman M, Heikkala J, Lappalainen K. (2000) Modeling, measurement and error compensation of multi-axis machine tools. Part I: theory. International Journal of Machine Tools and Manufacture,40:1535-1546. doi: https://doi.org/10.1016/S0890-6955(99)00101-7

[15] Ratchev S, Liu S, Huang W, Becker AA. (2006) An advanced FEA based force induced error compensation strategy in milling. International Journal of Machine Tools and Manufacture,46:542-551. doi: https://doi.org/10.1016/j.ijmachtools.2005.06.003

[16] Guo H, Zuo DW, Wu HB, Xu F, Tong GQ. (2009) Prediction on milling distortion for aero-multi-frame parts. Materials Science & Engineering A,499:230-233. doi: https://doi.org/10.1016/j.msea.2007.11.137

[17] Zhang J, Lin B, Fei J, Huang T, Xiao J, Zhang X, Ji C. (2018) Modeling and experimental validation for surface error caused by axial cutting force in end-milling process. The International Journal of Advanced Manufacturing Technology,99:327-335. doi: https://doi.org/10.1007/s00170-018-2468-x

[18] Khandagale P, Bhakar G, Kartik V, Joshi SS. (2018) Modelling time-domain vibratory deflection response of thin-walled cantilever workpieces during flank milling. Journal of Manufacturing Processes,33:278-290. doi: https://doi.org/10.1016/j.jmapro.2018.05.011

[19] Zozulya VV, Cartmell S, Basak TK. (2011) Numerical Solution of the Kirchhoff Plate Bending Problem with BEM. ISRN Mechanical Engineering,2011:295904. doi: https://doi.org/10.5402/2011/295904

[20] Ritz W. (1909) Theorie der Transversalschwingungen einer quadratischen Platte mit freien Rändern. Annalen Der Physik,333:737-786. doi: https://doi.org/10.1002/andp.19093330403

[21] M S, Poruba Z, L E, M A. (2020) Increasing the Accuracy of Free-Form Surface Multiaxis Milling. Materials,14:25. doi: https://doi.org/10.3390/ma14010025

Figures

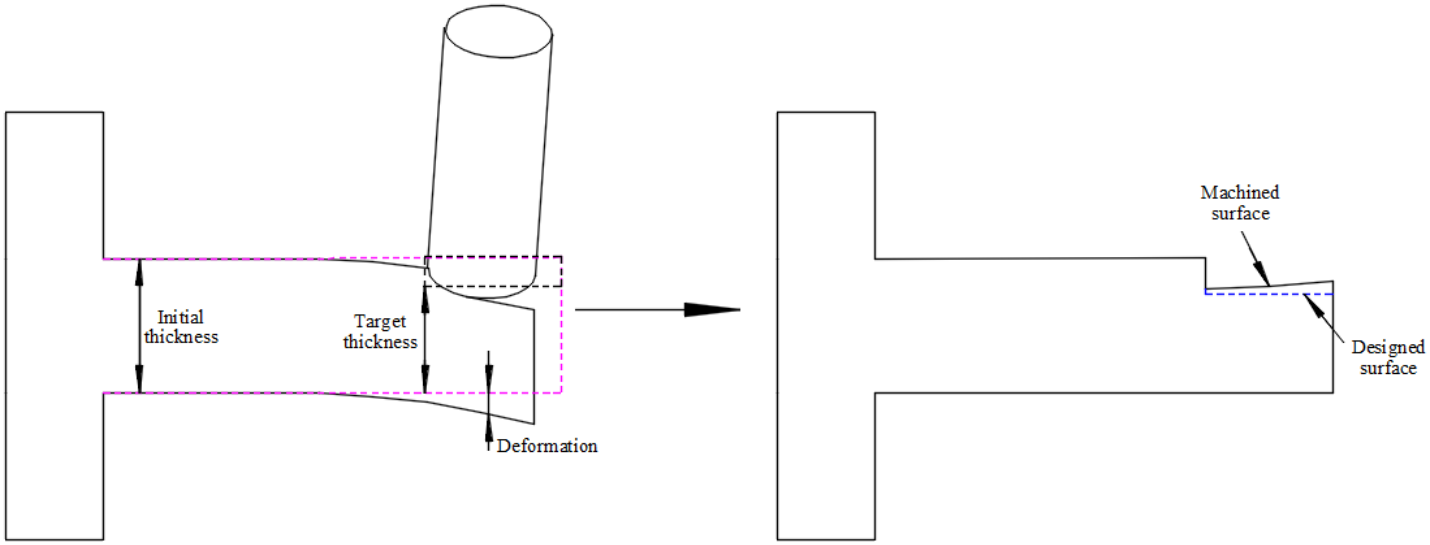

Figure 1

Deformation and surface error during thin-wall parts machining.

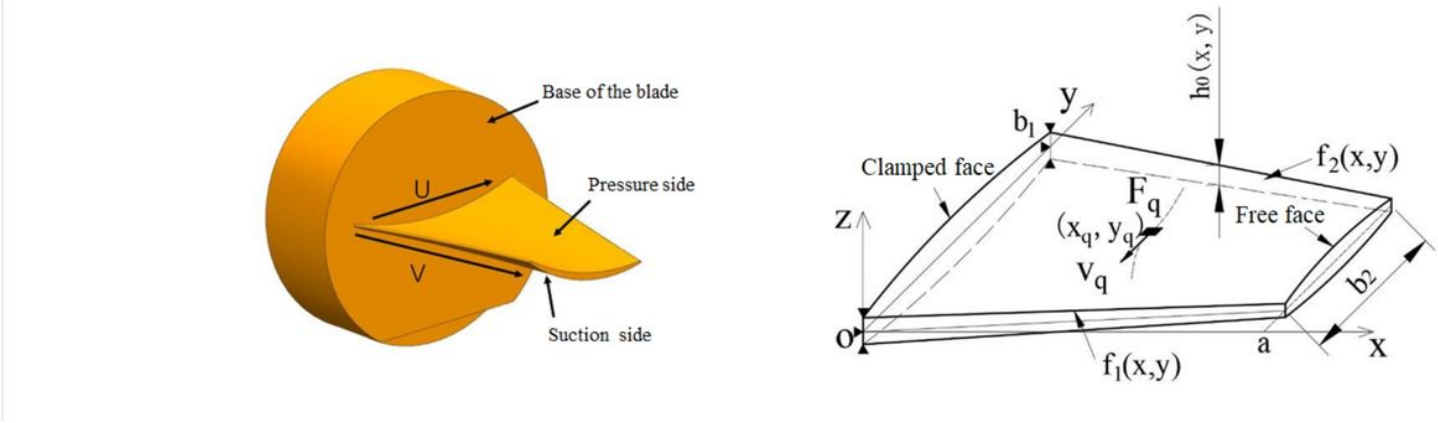

Figure 2

Blade model and its simplification

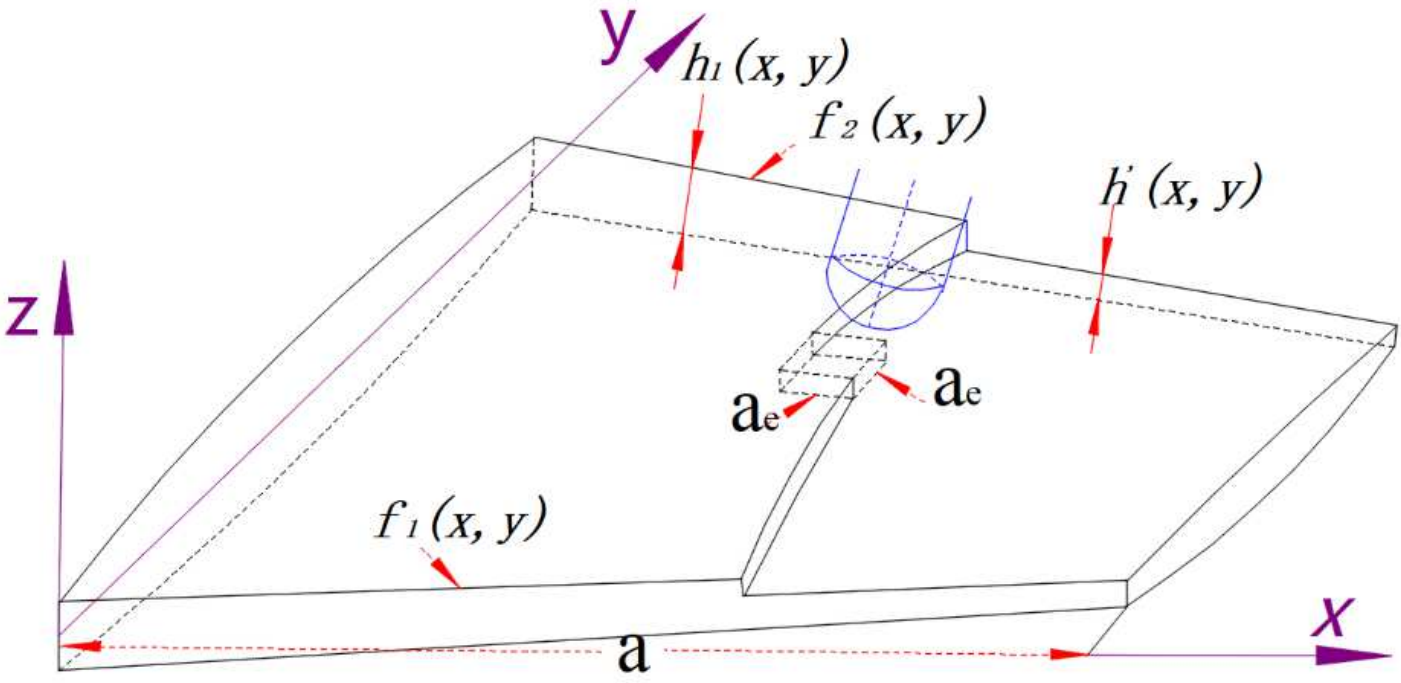

Figure 3

Diagram of deformation in simplified blade machining.

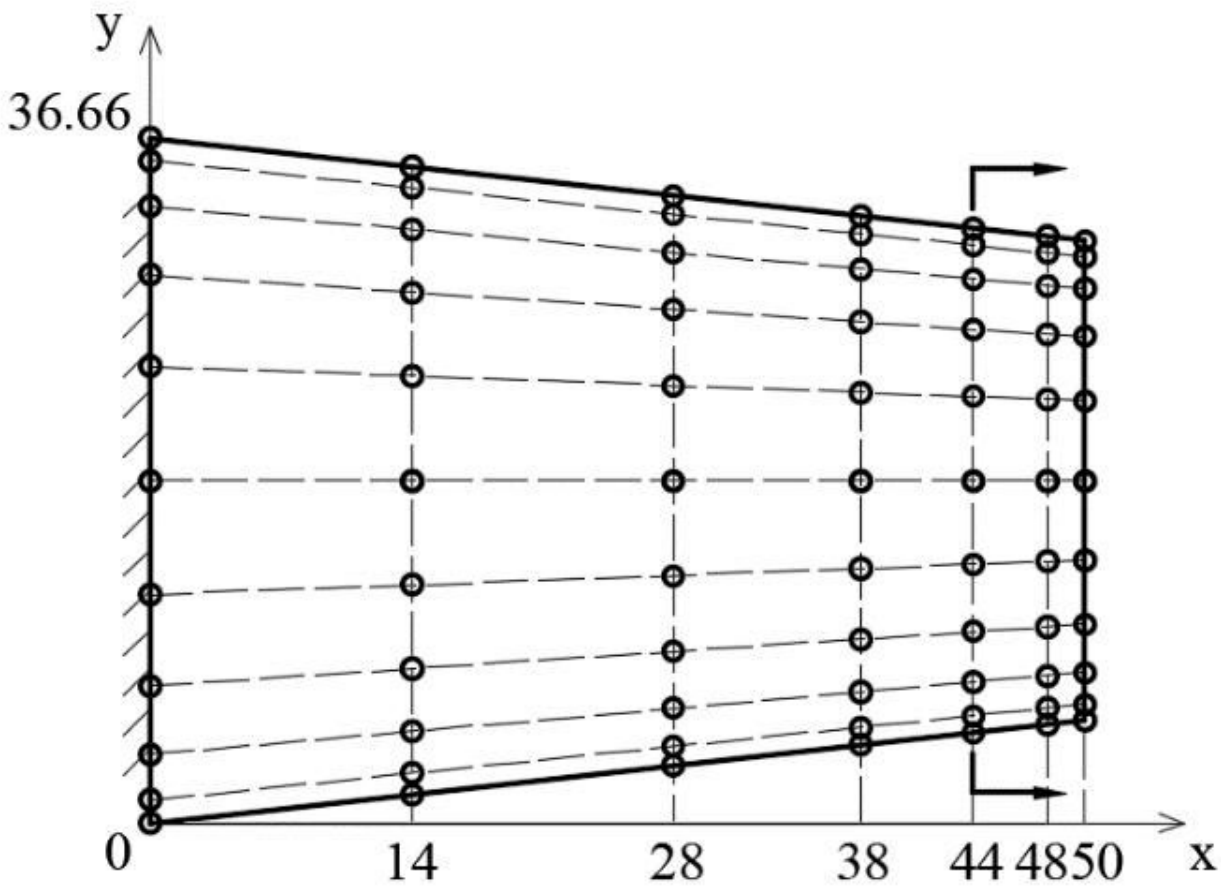

Figure 4

Diagram of thickness in simplified blade.

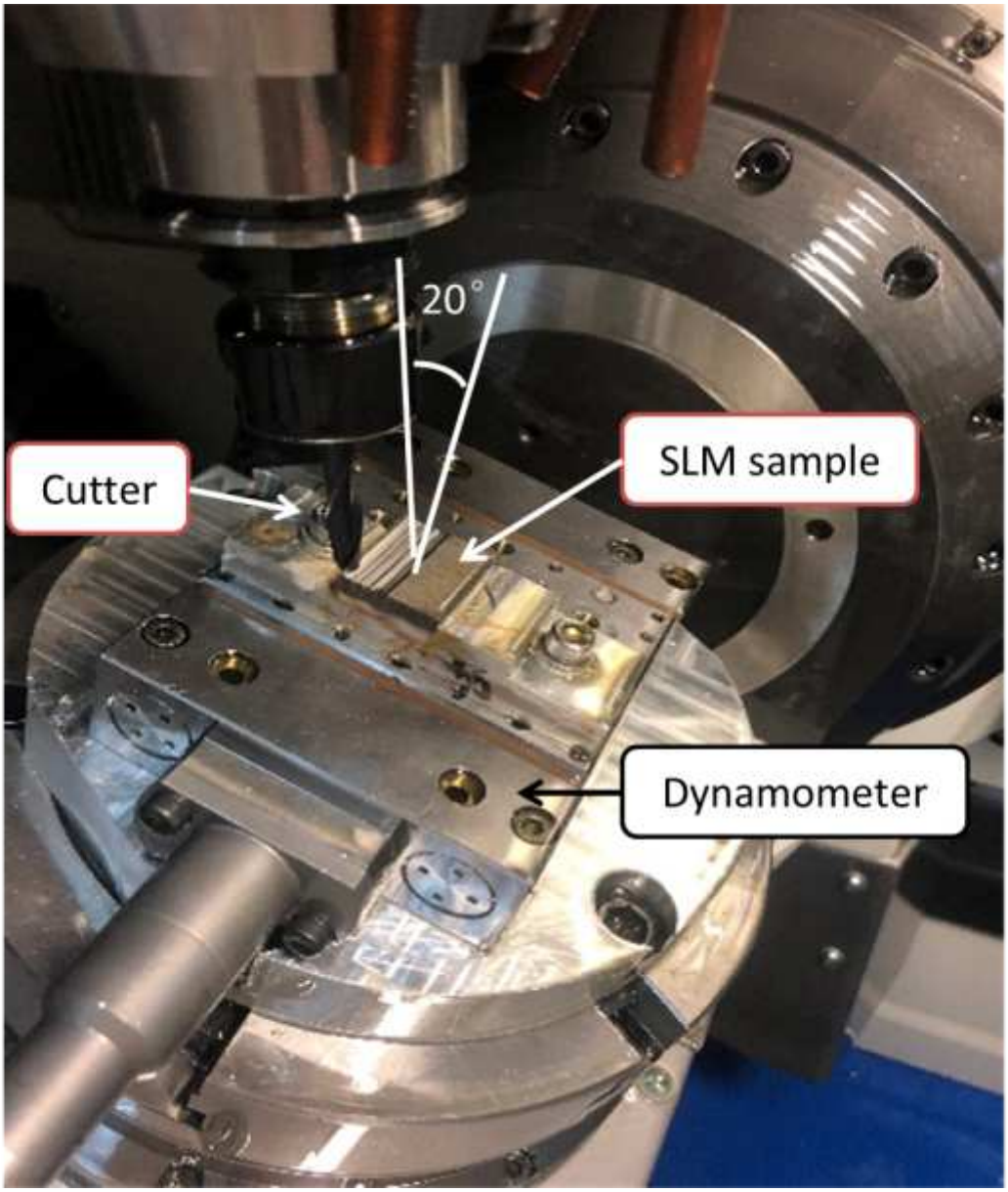

Figure 5

Machining force measurement process.

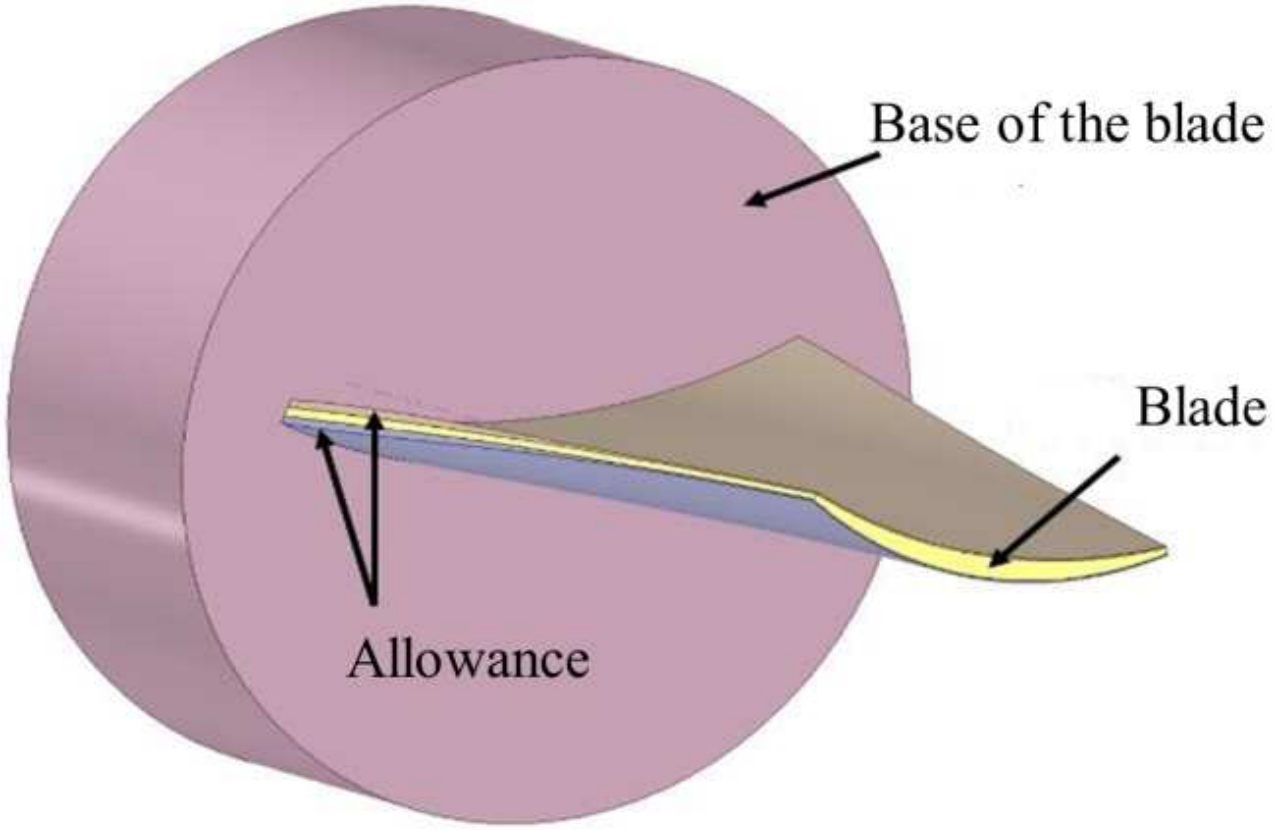

Figure 6

Model of semi-finished workpiece with Ritz non-uniform allowance.

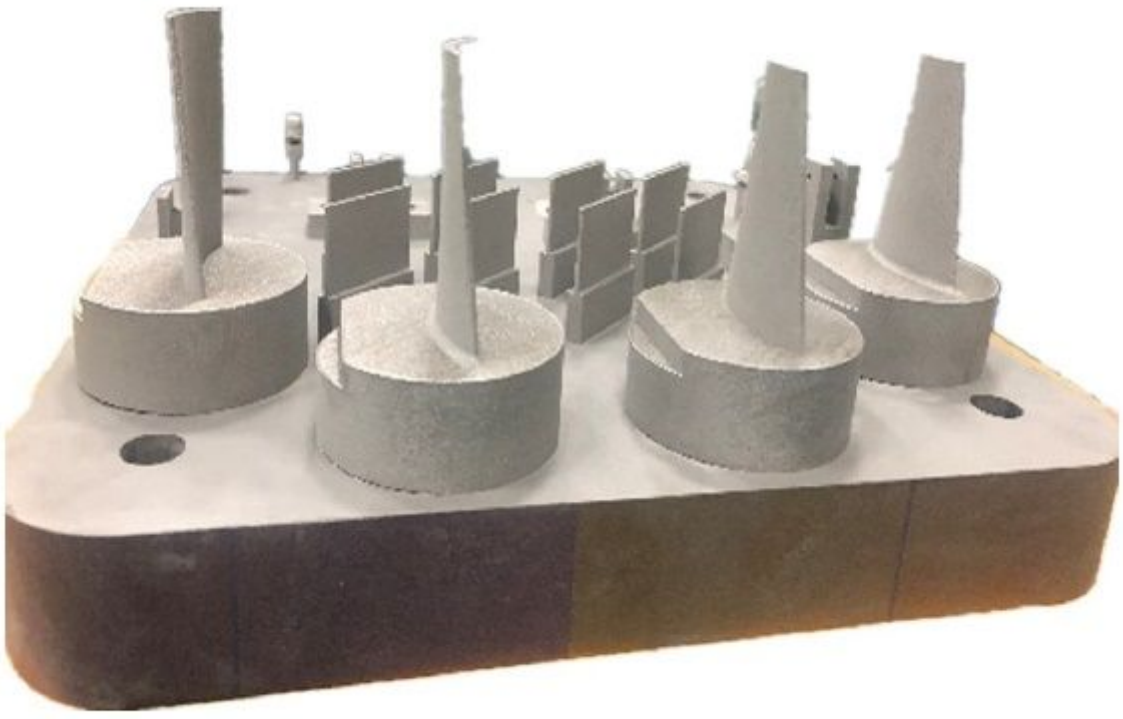

Figure 7

Blade samples fabricated by SLM.

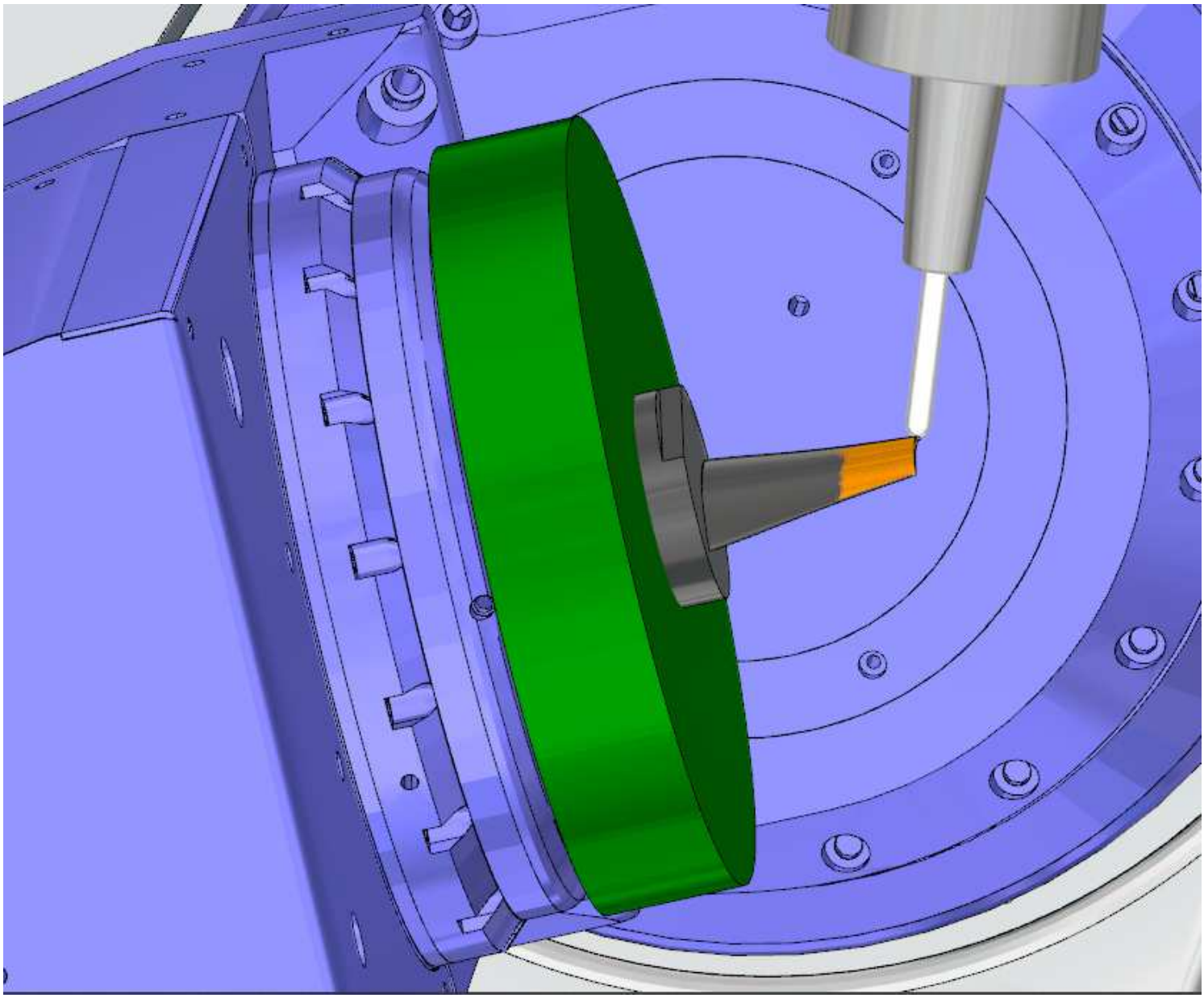

Figure 8

Diagram of 5-axis milling.

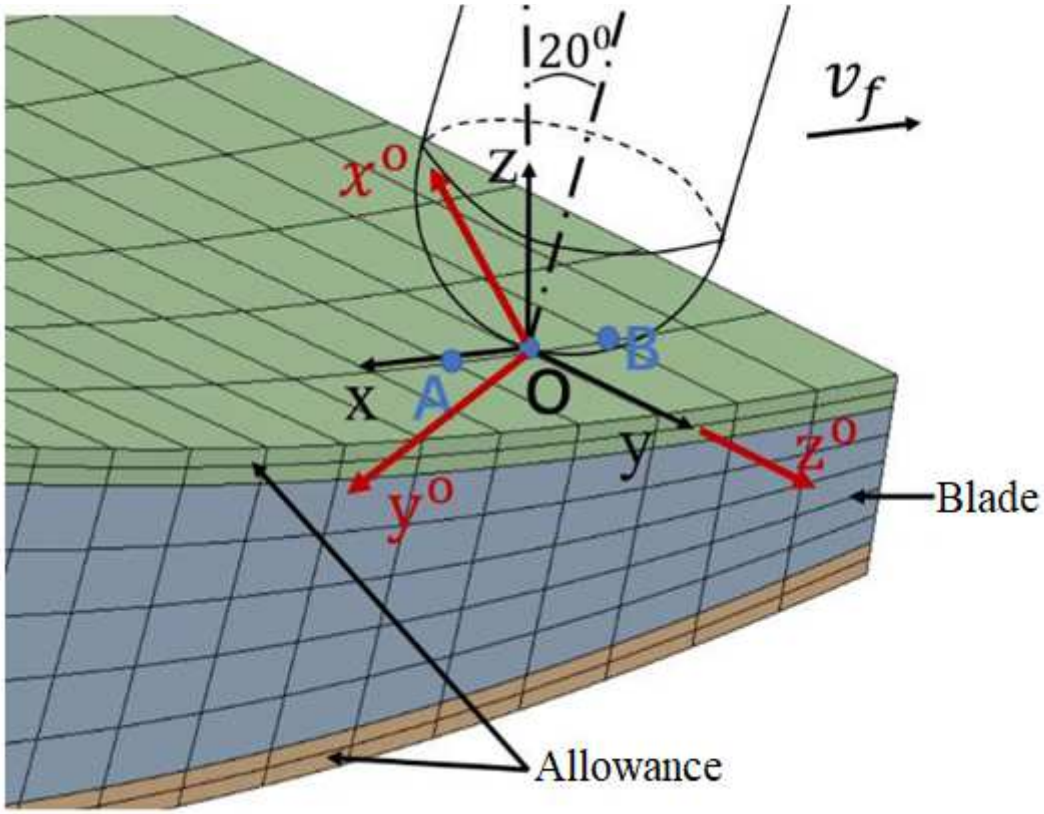

Figure 9

Diagram of coordinate transformation.

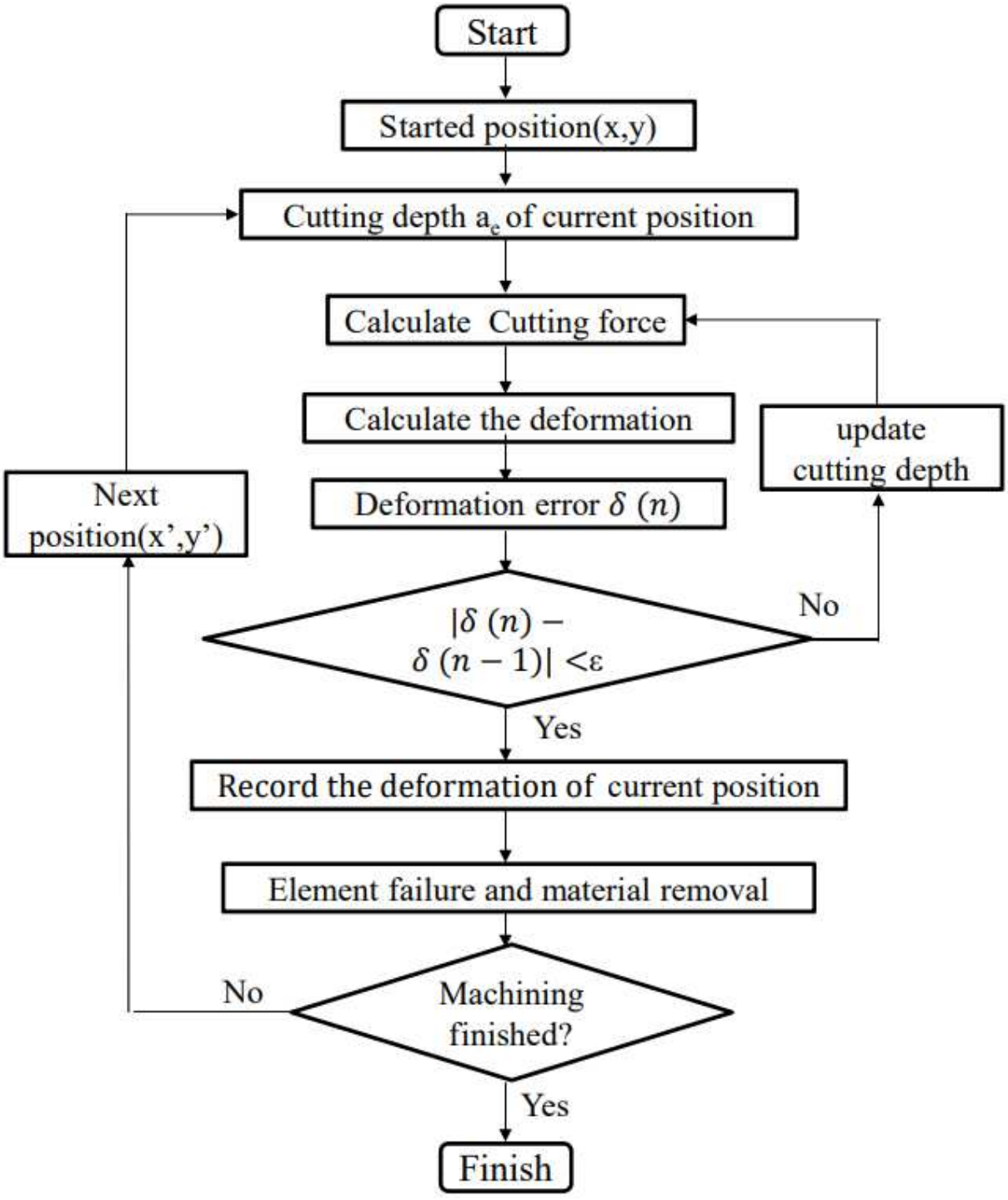

Figure 10

Flow chart of finite element analysis.

Figure 11

Blade samples after SLM. (a) Blade before machining, (b) Machined blade with Ritz allowance, (c) Machined blade with uniform allowance

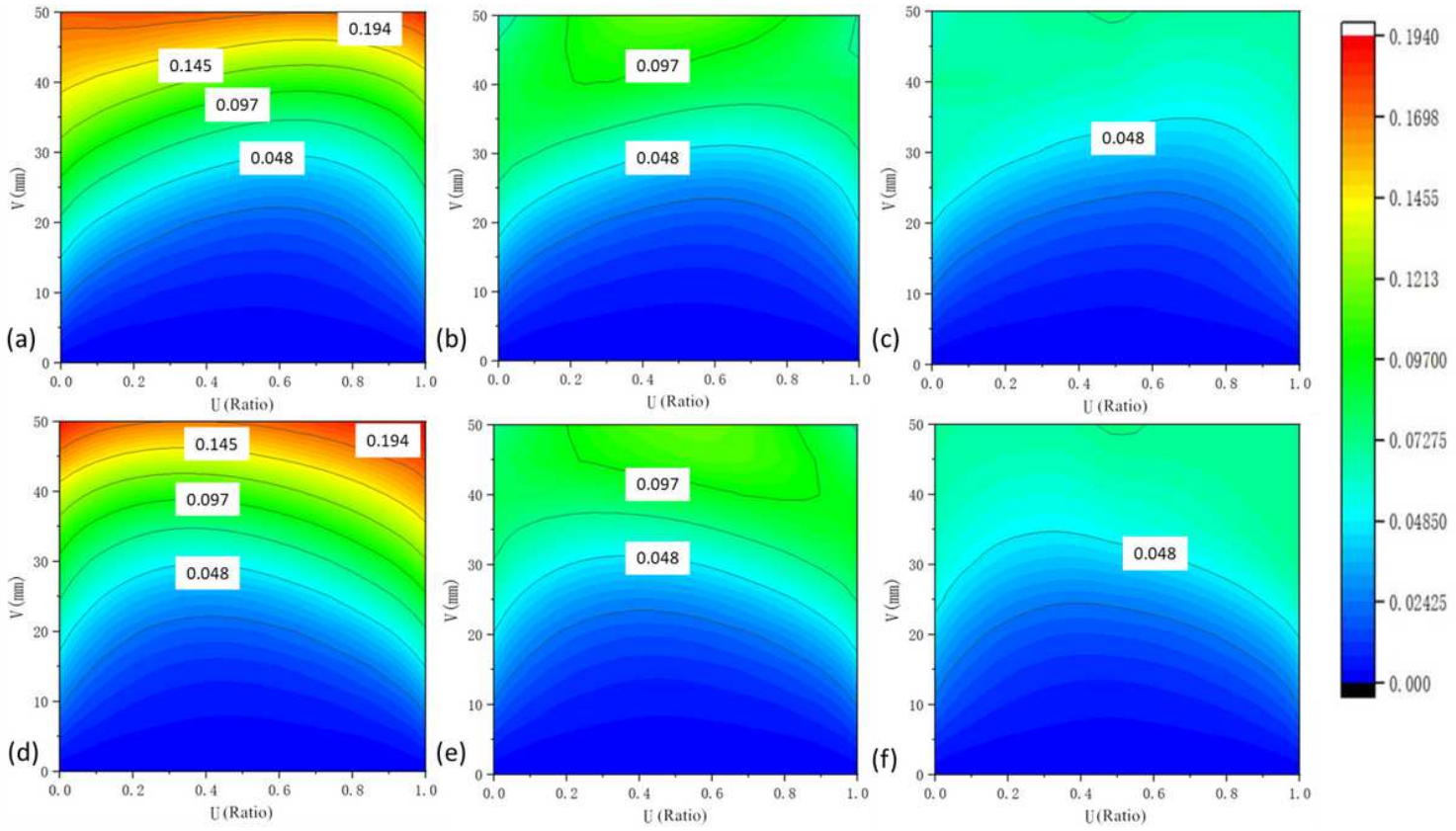

Figure 12

Residual error of machined blade with 3 different allowances. (a) pressure error with uniform allowance (d) suction back error with uniform allowance, (b) pressure error with sinuous allowance, (e) suction error with sinuous allowance, (c) pressure error with Ritz allowance, (f) suction error with Ritz allowance.

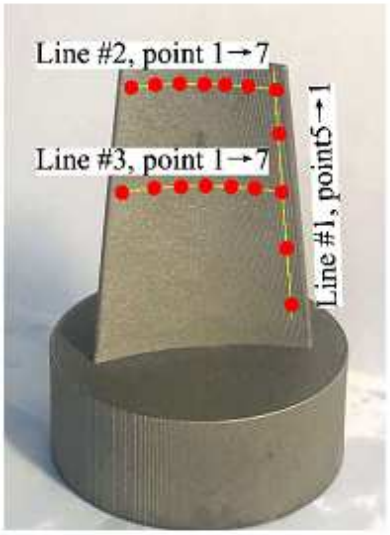

a) Schematic diagram of measure points.

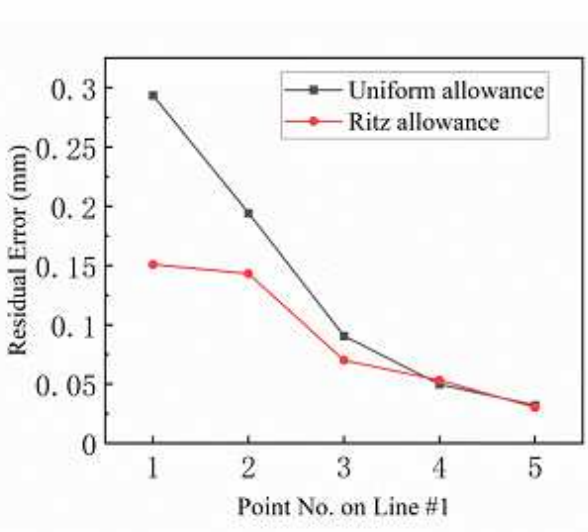

b) Results of line #1.

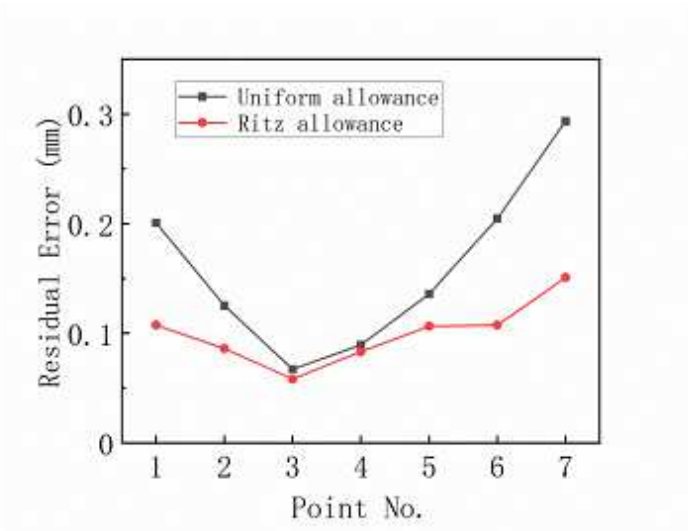

c) Results of line #2.

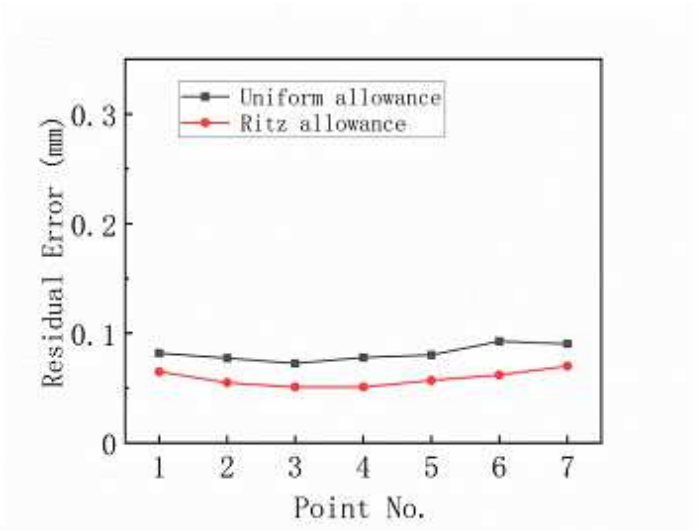

d) Results of line #3

Figure 13

Comparison of surface errors for milling of blades with uniform allowance and Ritz allowance.

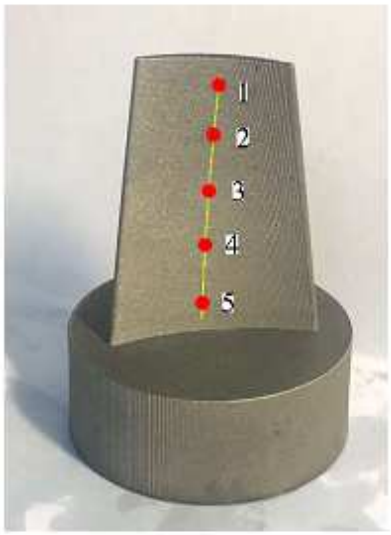

a) Schematic diagram of measure points

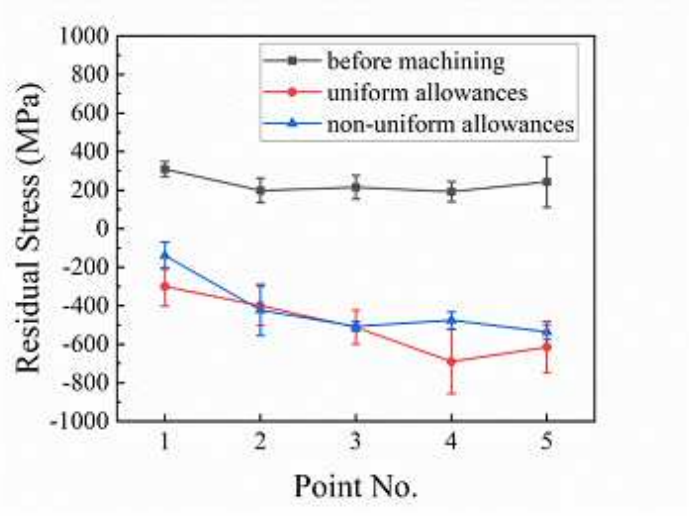

b) Residual stress results of pitched points

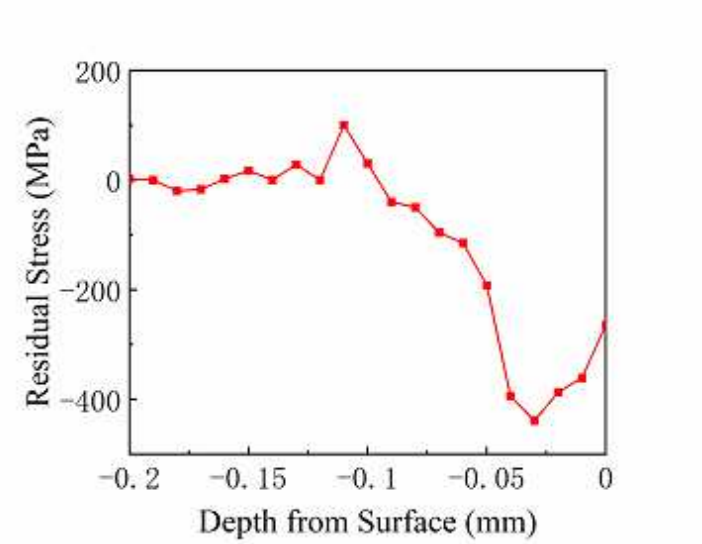

c) Residual stress results of pitched points along depth

Figure 14

Residual stresses of blade with Ritz allowance after machined.